Applied Catalysis B: Environmental 111–112 (2012) 571–577

Contents lists available at SciVerse ScienceDirect

Applied Catalysis B: Environmental

journal homepage: www.elsevier.com/locate/apcatb

A hierarchically structured and multifunctional membrane for water treatment

Hongwei Bai, Zhaoyang Liu*, Darren Delai Sun*

School of Civil & Environmental Engineering, Nanyang Technological University, Singapore 639798, Singapore

ARTICLE INFO

Article history:
Received 14 August 2011
Received in revised form 2 November 2011
Accepted 3 November 2011
Available online 12 November 2011

Keywords:
Antibacterial
Hierarchical
Membrane
Photocatalytic activity
Permeate flux

ABSTRACT

Currently, the biggest challenge for filtration membrane application is the severe membrane fouling problem, which consequently results in low flux and high energy cost. Herein, a novel kind of multifunctional membrane was fabricated via integrating the advantages of conventional polymer membrane as supporting layer and "forest" like hierarchically structured TiO_2/ZnO nanomaterials as functional layer. This membrane has shown multifunctional properties, such as, high photocatalytic activity, high flux and high antibacterial capacity, which make it as a good candidate to tackle the challenge of producing clean water at a constant high flux with no membrane fouling problem and energy saving manner. The outstanding performance of this novel membrane would bring enough benefits to filtration membrane industry for clean water production and environmental protection.

© 2011 Elsevier B.V. All rights reserved.

1. Introduction

More than one billion people over the world can't get to clean water due to the water quality deterioration and water resource scarcity [1,2]. The rapid industrialization and the successive emergence of unpredictable microorganisms has been contaminating the water bodies at an unprecedented rate [2]. What's more, the climate change has a great potential to worsen this trend [3,4]. There is an urgent need to develop a new cost effective and environmental friendly technology to counter the rising problem of drinking water shortage. Generally, water purification has two main tasks: decontamination and disinfection [5]. Compared with conventional activated sludge process, membrane filtration proved to be one of the most promising technologies to concurrently eliminate contaminants and bacteria to guarantee plenty of safe and clean water access to increasing number of people throughout the world [2,6]. An ideal membrane is featured in terms of high permeate flux, no membrane fouling and low energy consumption [6]. Membrane filtration has been widely used for clean water production, especially low-pressure driven membrane (MF/UF) is believed to have a promising prospect due to its relative low energy consumption [7,8]. Currently, polymer membrane dominates the market of membrane technology because of its flexibility, easy scale-up production etc. [7,8], but membrane fouling resulted from the adsorption/desorption of rejected inorganic, organic contaminants and bacteria greatly limits the broad application of membrane through reducing the flux, increasing the energy consumption, and shortening membrane lifespan [9]. Most of the MF/UF membrane is reported to be able to reject the bacteria, but the accumulated bacteria on membrane are still alive and would damage the polymer membrane surfaces, or cause other unexpected problems [10,11]. This obstacle, combined with its low flux, paints an image of being 'energy expensive' for membrane filtration. In the past decades, lots of attention has been stressed on the mitigation of membrane fouling, for example, backwashing and chemical agents [12] were used to clean away the accumulated pollutants; conventional coagulation processes [9] or powder activated carbon (PAC) adsorption [13] were introduced as a pretreatment to reduce the fouling potential, etc. But their disadvantages are the harm to the flux and lifespan of the membranes, causing secondary pollutants and increasing the operational costs [12]. It is our dream to fabricate a unique kind of multifunctional membrane to purify the polluted water in an environmental friendly and energy saving manner.

Titanium dioxide (TiO_2) and zinc oxide (ZnO), two kinds of popularly used semiconductive materials [14], have been widely applied in a lot of fields such as photocatalysis, electrochromic, photovoltaic, dye sensitized solar cells (DSSCs), sensor, energy storage and transfer, etc. [14–24], due to their unique electronic, magnetic, optical, chemical and mechanical properties. Especially, TiO_2 and ZnO based photocatalysts demonstrates excellent photodegradation ability of contaminants for water purification [23]. However, the use of TiO_2 or ZnO nanomaterials has the inherent and significant drawbacks, that are, the recombination of charge carriers (photogenerated electron–hole pairs) and the separation of used TiO_2 or ZnO nanomaterials from treated water [14].

In recent years, semiconductive materials, hierarchically structured architecture with a multi-scale organization, is demonstrated

* Corresponding authors.
E-mail addresses: baih0003@ntu.edu.sg (H. Bai), zyliu@ntu.edu.sg (Z. Liu), ddsun@ntu.edu.sg (D.D. Sun).

0926-3373/$ – see front matter © 2011 Elsevier B.V. All rights reserved.
doi:10.1016/j.apcatb.2011.11.009

to be able to maximize the photocatalytic activity by creating multi-scaled channels which are convenient for light scattering and mass transfer, and by providing larger surface area for pollutants access [17]. What's more, it is interesting to note that hierarchically structured semiconductor oxides with two different oxides are capable to inhibit the recombination of charge carriers [14], an unavoidable puzzle for single semiconductive material used for photocatalysis [25]. It is a practicable way to fabricate one kind of unique multifunctional membrane to integrate the common characteristics of polymer membrane and inorganic functional materials to create a no fouling, high flux and high antibacterial capacity membrane.

Here, for the first time, a novel kind of multifunctional membrane was fabricated via integrating the advantages of conventional polymer membrane as supporting layer and "forest" like hierarchically structured TiO_2/ZnO nanomaterials as functional layer. This novel membrane possesses the common advantages of polymer membrane and multifunctional properties of the hierarchical TiO_2 nanofiber/ZnO nanorod materials, which demonstrated to be able to produce clean water at a constant high flux with no membrane fouling problem and energy saving manner.

2. Experimental

2.1. Fabrication of TiO_2 nanofiber by electrospinning method

Dissolved 6 wt% polyvinylpyrrolidone (PVP Mn 1,300,000, Aldrich) in the mixture of absolute ethanol and acetone (V/V = 4:1) solution, then added 20 wt.% $Ti(OBu)_4$ and stirred to form a clear sol–gel solution ready for electrospinning TiO_2 nanofiber [14,26].

The electrospinning setup for fabrication of TiO_2 nanofiber was similar to that previously reported [14,26], and the scheme was drawn as Fig. S1 shown. Here, a plastic capillary with an inner diameter of 0.5 mm was used as the spinneret with a spinning speed of 5–10 μL/min. At an applied high voltage of 15–19 kV, a non-woven mat of PVP/$Ti(OBu)_4$ composite was collected on a grounded aluminum foil at an electrode distance of 18 cm. The as-spun nanofibers were then calcined at 550 °C in air for 1 h, with a temperature rise step at 2 °C/min.

2.2. Synthesis of TiO_2 nanofiber/ZnO nanorod materials

100 mg as-spun TiO_2 nanofibers were suspended in an aqueous solution (100 mL) of Zinc acetate hydrate (0.03 M) and hexamethylenetetramine (HMTA: $C_6H_{12}N_4$), and was ultra-sonicated for 10 min. Then the well-dispersed mixture was hydrothermally treated for 6–10 h at 95 °C in an electric oven [22,27]. Through adjusting the amount of TiO_2 nanofibers in the aqueous solution of zinc acetate hydrate and hexamethylenetetramine, the molar ratio of Ti:Zn in the final TiO_2 nanofiber/ZnO nanorod materials can be tuned.

During the reaction period, it has been suggested the following formation process of ZnO nanorods:

$$(CH_2)_6N_4 + 6H_2O = 6HCHO + 4NH_3$$

$$NH_3 + H_2O = NH_4^+ + OH^-$$

$$2OH^- + Zn^{2+} = ZnO + H_2O$$

While the ZnO nucleated on the rough knots of TiO_2 nanofiber surface and grew outwardly till forming an integrate nanorod.

As a reference, ZnO nanorods without the addition of TiO_2 nanofibers were also synthesized using the same methods as above.

2.3. Assembly of the novel membrane with "forest" like hierarchically structured functional layer

100 mg successfully as-synthesized TiO_2 nanofiber/ZnO nanorod hierarchical materials were uniformly assembled on one piece of commercial cellulose acetate membrane (Millipore membrane discs Ø 47 mm, 0.20 μm), which was properly mounted at the bottom of filtration cup (Fig. S2). Then the filtration cup was filled with deionized (DI) water and slowly switched on the N_2 gas valve to provide pressure, as a result of the combined action of water and regularly discharged N_2 gas, the TiO_2 nanofiber/ZnO nanorod hierarchical materials were uniformly assembled on the cellulose acetate membrane and were compressed to form a novel membrane with a "forest" like hierarchically structured functional layer. This novel membrane was assembled and characterized successfully. It was used to do further application test to evaluate its flux performance and photocatalytic oxidation activity.

As a comparison, using the above mentioned method, 100 mg TiO_2 P25 was also deposited on another piece of commercial cellulose acetate membrane to form a TiO_2 P25 deposited membrane, which was characterized and used for further application test such as flux performance investigation.

2.4. Characterization

The structure and crystal phase of the TiO_2 nanofiber/ZnO nanorod materials were examined using Shimadzu XRD-6000 X-ray diffractometer with monochromated high-intensity Cu Kα radiation (λ = 1.5418 Å) operated at 40 kV and 30 mA. The scanning rate was 2°/min.

The morphologies of TiO_2 nanofiber/ZnO nanorod hierarchical materials and the novel membrane were observed by field-emission scanning electron microscopy (FESEM, Jeol JSM-6340F) and transmission electron microscopy (TEM, Jeol JEM-2010). Energy dispersive X-ray (EDS) measurement was conducted using the EDAX system attached to the same field emission scanning electron microscopy with carbon tape and gold sputtering used for the sample preparations.

BET specific surface area of the novel membrane was determined at liquid nitrogen temperature (77 K) using a Micromeritics ASAP 2040 system. Before the measurement, 0.1 g sample was outgassed under vacuum for 10 h at 250 °C.

The UV–visible adsorption values of the synthesized TiO_2 nanofiber/ZnO nanorod materials, the adsorption value of methyl blue (MB), humic acid (HA) were measured by the UV–visible spectrophotometer (UV–visible resource 3000). The total organic carbon (TOC) of HA was measured by a TOC analyzer (TOC-V CSH Shimadzu).

2.5. Concurrent photocatalytic oxidation and membrane filtration

After the novel membrane was assembled via a dead-end apparatus, as shown in Fig. 1 which has been reported by us previously [23,28] was used for the investigation of concurrent photocatalytic oxidation and membrane filtration. In this concurrent processes, a specific Upland UVP lamp (254 nm, 40 mW/cm^2), equipped with a specific power source, was suspended above the novel membrane.

For the photodegradation of MB, 60 mL MB solution with an initial concentration of 50 mg/L was filled into the filtration cup. The MB solution in the filtration cup was kept in the dark for 1 h to ensure the adsorption equilibrium had been reached and then turned on the UV light and the transmembrane pressure (TMP). The TMP was maintained around 0.05 MPa during the whole processes. 3 mL permeate was collected to measure the UV-adsorption value at 605 nm (the major adsorption peak of herein used MB, is around 605) at 10 min, 20 min, and 30 min. As

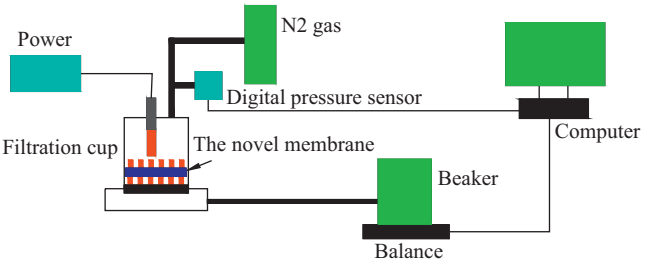

Fig. 1. Illustrated scheme of the concurrent photocatalytic oxidation and membrane filtration.

a contrast, the photodegradation of MB by TiO_2 P25 deposited membrane was also conducted simultaneously.

For the photodegradation of HA, 60 mL HA solution with an initial concentration of 30 mg/L was filled into the filtration cup. The filtration cup with HA solution was kept in the dark for 2 h to ensure the adsorption equilibrium had been reached and then turned on the UV light and the transmembrane pressure (TMP). TMP was maintained around 0.05 MPa during the whole processes. 3 mL permeate was collected to measure the UV-adsorption value at 436 nm at 20 min, 40 min, and 60 min. As a contrast, the photodegradation of HA by TiO_2 P25 deposited membrane was also conducted simultaneously.

The photocatalytic degradation of MB/HA as a function of the irradiation time in the presence of the novel membrane or TiO_2 P25 deposited membrane was observed to follow first-order kinetic reaction. Thus, the photocatalytic reaction can simply be described by:

$$r = \frac{-d[\boldsymbol{c}]}{dt} = k[\boldsymbol{c}] \quad (1)$$

or

$$\frac{-\ln[\boldsymbol{c}]}{c_0} = kt \quad (2)$$

where r is the degradation rate of MB or HA, $[\boldsymbol{c}]$ is the concentration of MB or HA, c_0 is initial concentration of MB or HA, t is the irradiation time, and k is the first order kinetic reaction rate constant [23,28].

2.6. Investigation of membrane flux performance

Besides the investigation of photocatalytic activity, the flux performance of the novel membrane and TiO_2 P25 deposited membrane over TMP was also investigated in the same dead-end apparatus as shown in Fig. S2 without the UV light irradiation. This bench-scale system comprised of a membrane cell with a filtration cup volume of 60 mL, which housed the novel membrane. The effective membrane area was 13.4 cm^2. Pressure was provided by a compressed N_2 gas cylinder that was connected to the filtration cup. Permeate was collected and its mass was measured continuously over time using a weighing balance connected to a data logger. Data were collected on a per second basis and averaged per minute. Permeate flux was calculated on the basis of permeate mass divided by effective surface area and filtration time, unit is L/(m^2 h). For the evaluation of membrane flux performance, at the steady state of a given TMP, average permeate flux was measured. As a contrast, using the same method, the membrane flux of TiO_2 P25 deposited membrane was also evaluated and the corresponding permeate flux at different TMP was calculated and recorded. Finally, the relationship between permeate flux and TMP for the novel membrane and P25 deposited membrane were drawn and displayed in Fig. 6a.

2.7. Investigation of the anti-fouling capacity

100 mg TiO_2 nanofiber/ZnO nanorod hierarchical materials were assembled on one piece of polymer membrane; the concentration of initial HA feed water was 30 mg/L; and the photocatalytic reaction time was 30 min. The HA removal rate was measured under different permeate flux. The relationship between permeate flux and HA removal rate was delineated in Fig. 6b. As a reference, the anti-fouling capacity of TiO_2 P25 membrane was also investigated and shown in Fig. 6b.

2.8. Anti-bacterial test

The anti-bacterial properties of the synthesized TiO_2 nanofiber/ZnO nanorod hierarchical materials were investigated by inhibition testing. Nutrient agar was poured into disposable sterilized Petri dishes and allowed to solidify. 100 μL of *Escherichia coli* bacterial solution (10^6 CFU/mL) were streaked uniformly over each plate. Identical amount of the synthesized TiO_2 nanofiber/ZnO nanorod hierarchical materials, as-spun TiO_2 nanofiber and TiO_2 P25 were gently placed on the solidified agar gel in separate Petri dishes [19]. Then the plates were incubated at 37 °C for 24 h. The result of TiO_2 nanofiber/ZnO nanorod hierarchical materials was shown in Fig. 7, while the result of TiO_2 nanofiber and TiO_2 P25 were shown in Fig. S4.

3. Results and discussion

Herein for the first time, we report a novel kind of membrane, in which the "forest" like functional layer is hierarchically constructed by TiO_2 nanofiber/ZnO nanorod hierarchical materials, that is, TiO_2 nanofiber as trunk and ZnO nanorod as branch. This novel hierarchical membrane possesses the following advantages: [19,23,29–34] (1) high permeate flux; (2) no membrane fouling; and (3) high antibacterial capacity without UV light. All the above advantages are all because of the special structure and component of the TiO_2 nanofiber/ZnO nanorod hierarchical materials, which provide: [17,31–34] (i) large specific surface area for photocatalytic reaction, (ii) hierarchical pores for easy mass transfer and efficient light harvesting, and (iii) retardation of the recombination of photogenerated charge carriers. We will discuss the details in the below paragraphs. As a comparison, the commercial TiO_2 Degussa P25 powder (average particle size: 25 nm) was also assembled on the polymer membrane with the same method as the novel membrane.

The morphologies of the electrospun TiO_2 nanofiber, and the TiO_2 nanofiber/ZnO nanorod hierarchical materials were characterized by field emission scanning electron microscopy (FESEM) in Fig. 2a–c, respectively. It can be seen that the electrospun TiO_2 nanofiber has a length of 100 μm to 1 cm and a diameter of 400–800 nm (Fig. 2a). After hydrothermally treated, well tailored ZnO nanorods with diameters of 100–300 nm perpendicularly grew on the surface of TiO_2 nanofibers. In this hierarchical structure, the TiO_2 nanofibers act as trunks and the ZnO nanorods act as branches [24]. This hierarchical structure was also observed by transmission electron microscopy (TEM), as shown in Fig. 2d, and high resolution transmission electron microscopy (HRTEM), as shown in Fig. 2e. Obviously, ZnO nanorods are rooted from the rough surfaces of TiO_2 nanofibers and grew outwardly into hexagonal rods. The lattice image and the selected area electron diffraction (SAED) pattern displayed in Fig. 2e can be identified with crystallographic planes of the ZnO wurtzite structure [34]. As the energy disperse spectrum (EDS) shown in Fig. 2f, the elements of Ti, Zn and O dominate the components of this hierarchical materials, wherein the Zn comes from ZnO nanorod, while Ti comes from TiO_2 nanofiber. And the XRD patterns in Fig. 3 revealed that the crystal phase of TiO_2

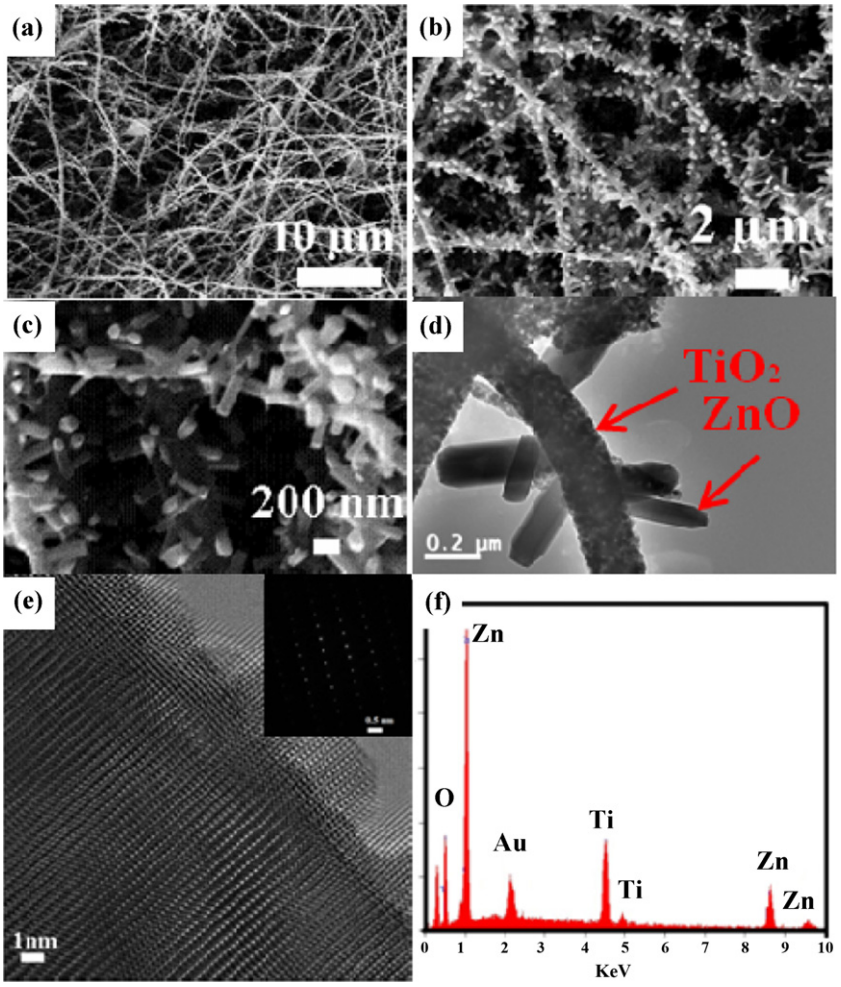

Fig. 2. SEM images of (a) electrospun TiO_2 nanofiber, (b) and (c) different magnifications of TiO_2 nanofiber/ZnO nanorod hierarchical materials, (d) TEM image of TiO_2 nanofiber/ZnO nanorod hierarchical materials, (e) HRTEM image of ZnO nanorod on TiO_2 nanofiber/ZnO nanorod hierarchical materials, insert was selected area electron diffraction (SAED) pattern, and (f) EDS spectrum of TiO_2 nanofiber/ZnO nanorod hierarchical materials.

nanofiber substrate was anatase phase, while ZnO nanorod was crystallized into hexagonal wurtzite phase. It is clear that this fabrication method successfully achieved a hierarchically structured wurtzite ZnO nanorod and anatase TiO_2 nanofiber.

After the novel membrane was compressively assembled, TiO_2 nanofiber/ZnO nanorod hierarchical materials formed a "forest" like hierarchical structure with a multi-scaled network, working as

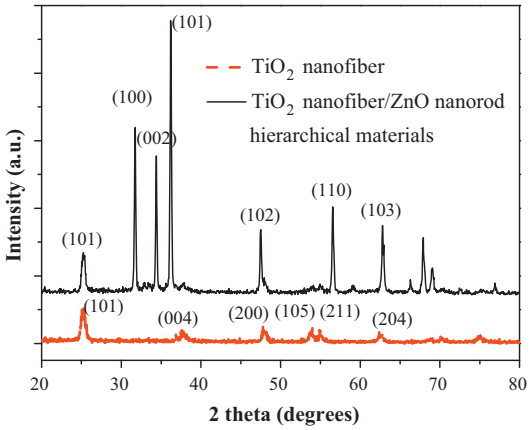

Fig. 3. XRD patterns of TiO_2 nanofiber and TiO_2 nanofiber/ZnO nanorod hierarchical materials.

the functional layer of the membrane, as shown in the schematic diagram and SEM image of Fig. 4a. On the contrary, a dense layer formed as the functional layer for P25 deposited membrane, as shown in the schematic diagram and SEM image of Fig. 4b. This 'forest' like functional layer formed by TiO_2 nanofiber/ZnO nanorod hierarchical materials is not only convenient for light harvesting and scattering, which was verified by the UV–visible spectrum, wherein TiO_2 nanofiber/ZnO nanorod hierarchical materials has an obvious red-shift toward the visible range in a comparison with P25 (Fig. 5); but also favorable for the mass transfer and enlarging the reaction sites [17,29], which was verified by the fact that the BET specific area of TiO_2 nanofiber/ZnO nanorod hierarchical materials was measured to be 89.67 m^2/g, much higher than that of P25 (34.38 m^2/g). Moreover, the two component structure of TiO_2 nanofiber/ZnO nanorod hierarchical materials is beneficial for the retardation of the generated electron–hole pairs by promoting the charges transfer between ZnO nanorods and TiO_2 nanofibers, as shown in Fig. 4c [21]. Hence, this structure has a great potential to enhance the photocatalytic activity.

The typical natural organic matter (NOM) in waters, such as HA, and the typical dye in industry, such as MB, were used as probe contaminants to investigate the performances of photocatalytic activity and membrane filtration of the novel membrane, with TiO_2 P25 deposited membrane as a comparison. With the same amount of catalysts and the same reaction conditions, the novel membrane demonstrated better removal rates of MB and HA than

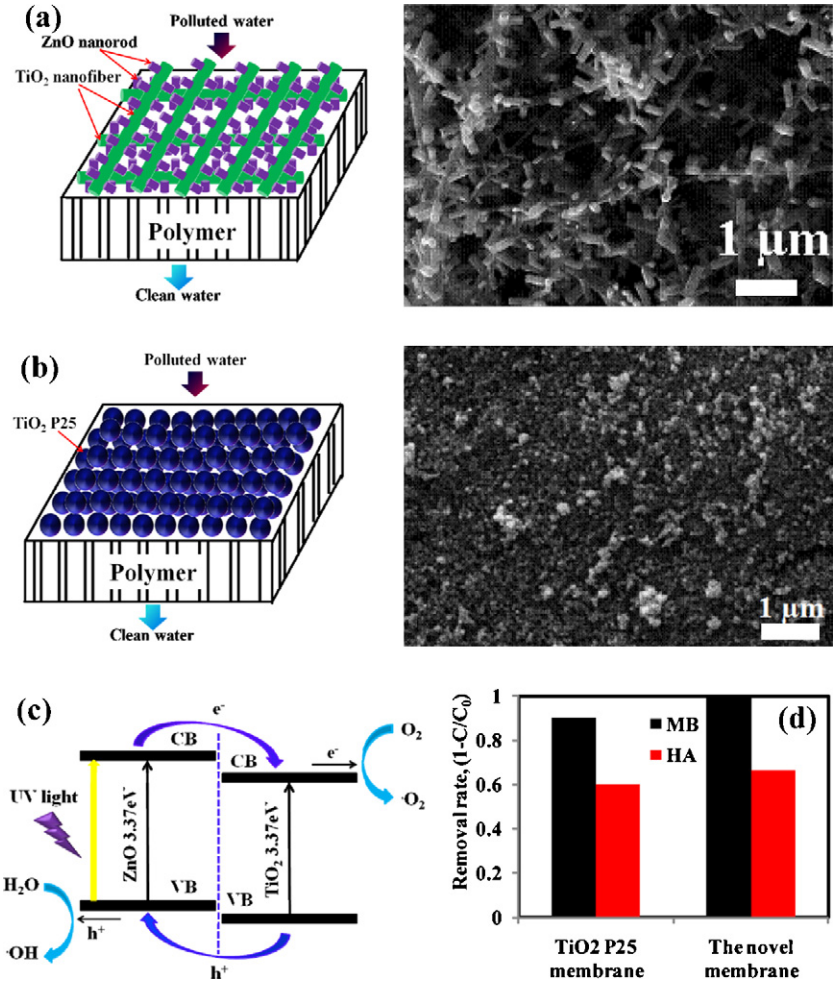

Fig. 4. (a) Left side is the schematic diagram of "forest" like hierarchically structured functional layer of the novel membrane, right side is its surface SEM image; (b) left side is the schematic diagram of dense functional layer of the P25 deposited membrane, right side is its surface SEM image; (c) schematic diagram showing the energy band structure and electron–hole pair separation in the TiO_2 nanofiber/ZnO nanorod hierarchical materials, and (d) MB and HA removal by the novel membrane and P25 deposited membrane.

P25 deposited membrane (Fig. 4d). And also the novel membrane showed a better TOC removal rate of HA, as shown in Fig. S3. The high photocatalytic activity is on the one hand to minimize the fouling formation, and on the other hand to ensure the constant high flux performance of membrane.

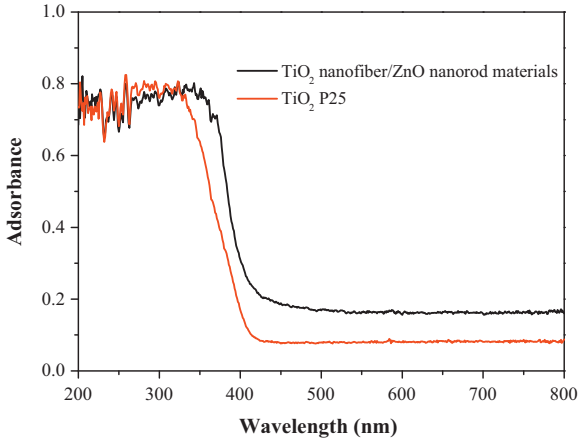

Fig. 5. UV–visible spectra of TiO_2 nanofiber/ZnO nanorod hierarchical materials and TiO_2 P25.

In addition to the photocatalytic activity, membrane filtration with flux performance was also investigated. The relationship between permeate flux and transmembrane pressure (TMP) was studied in Fig. 6a. Clearly, the hierarchical TiO_2 nanofiber/ZnO nanorod structure provides the multi-channeled functional layers on the polymer membrane surface, the permeate flux of which was proportional to TMP with a liner regression line ($R^2 = 0.987$), in contrast to the dense layer deposited by P25, the permeate flux of which was not fitted with a linear regression line ($R^2 = 0.770$) in Fig. 6a. Through observing the relationship between permeate flux and HA removal rate in a concurrent membrane filtration and photocatalysis system, the anti-fouling capacity of the novel membrane and TiO_2 P25 deposited membrane were investigated as shown in Fig. 6b. The experimental results demonstrated that HA removal rate generally decreased with the increase of permeate flux; but when the permeate flux was less than 11 L/m^2 h, the decrease of HA removal rate was not significant, which means that the flux of 11 L/m^2 h is the balance point between photocatalytic degradation of HA and flux under our experimental condition. When the permeate flux was larger than 11 L/m^2 h, a significant decrease of HA removal rate started, which means longer reaction time is needed to reach the same photodegradation effect at a given permeate flux condition. Similarly, it can be seen that the balance permeate flux for TiO_2 P25 deposited membrane is 7 L/m^2 h, which is smaller than that of the novel membrane. Therefore, it is reasonable to

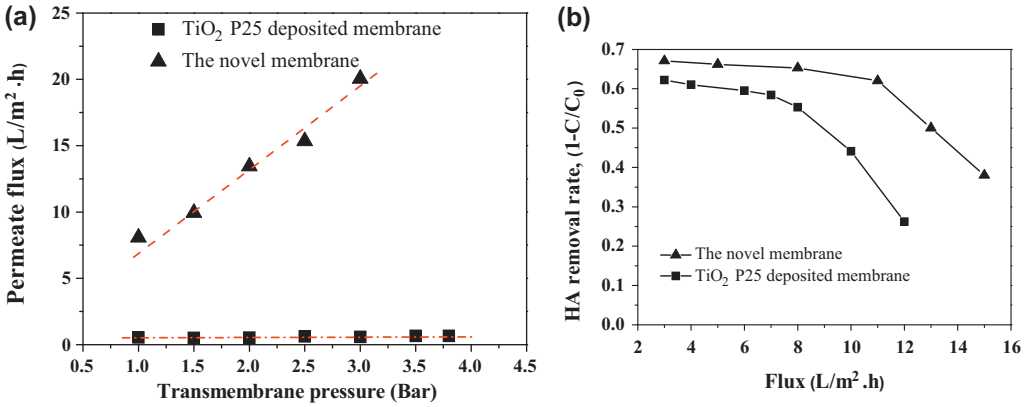

Fig. 6. (a) Permeate flux of the novel membrane and P25 deposited membrane as the function of transmembrane pressure (TMP), and (b) effect of the permeate flux on anti-fouling capacity of the novel membrane.

believe that this novel membrane can produce clean water at an industrially acceptable flux, no membrane fouling and low energy consumption rate (low TMP).

The TiO_2 nanofiber/ZnO nanorod hierarchical materials were also applied for antibacterial test. 100 μL of well-grew *E. coli* bacterial solution (10^6 CFU/mL) were streaked uniformly over each well solidified nutrient agar culture plate, then identical amount of TiO_2 nanofiber/ZnO nanorod hierarchical materials, TiO_2 nanofiber and P25 were placed in the center of the plates [19]. After overnight's incubation at 37 °C, the result of TiO_2 nanofiber/ZnO nanorod hierarchical materials was shown in Fig. 7. Obviously, a zone of inhibition appeared around the TiO_2 nanofiber/ZnO nanorod hierarchical materials (white area), but no obvious inhibition indication appeared to that of TiO_2 nanofiber and P25 (Fig. S4). This clearly indicated that the TiO_2 nanofiber/ZnO nanorod hierarchical materials also possess the antibacterial ability for water purification. The TiO_2 nanofiber/ZnO nanorod hierarchical materials exhibited higher antibacterial capacity than TiO_2 P25 because of its special hierarchical structure. The TiO_2 nanofiber/ZnO nanorod hierarchical materials enhance the photocatalytic activity owing to the specific hierarchical structure which would enlarge the specific surface area for mass transfer and providing more reaction sites; enhance the light absorption ability via allowing more light reflection and adsorption inside its interior; retard the recombination of photogenerated electrons and holes via promoting electrons transferring from ZnO to TiO_2 [21,33]. The enhanced photocatalytic activity of TiO_2 nanofiber/ZnO nanorod photocatalyst greatly benefits its antibacterial capacity. At the same time, the hierarchical TiO_2 nanofiber/ZnO nanorod photocatalysts would also promote the intact contact between bacteria and photocatalysts [35].

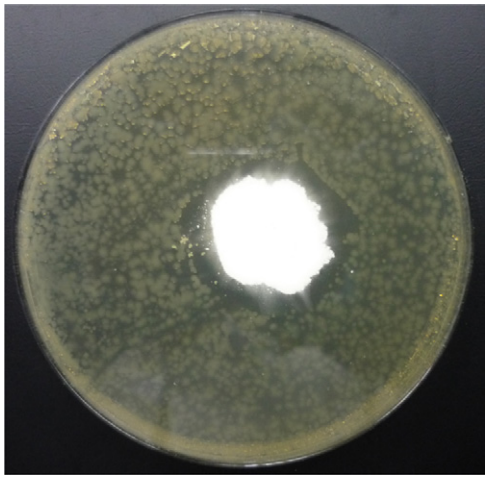

Fig. 7. The anti-bacterial test of TiO_2 nanofiber/ZnO nanorod hierarchical materials without UV irradiation.

4. Conclusion

In summary, a novel membrane with "forest" like hierarchically structured functional layer has been successfully assembled. This new kind of membrane possesses multi-advantages: high permeate flux and photodegradation capacity, no membrane fouling, and high antibacterial capacity. All of these advantages of this membrane can bring enormous benefits to the water purification field. This novel membrane possesses a potential to eliminate contaminants and bacteria concurrently in a no membrane fouling, high flux and energy saving manner.

Acknowledgments

We are grateful for the financial support received from the Prime Minister's Office of Singapore via an initiative called The Enterprise Challenge under award number P00579/1273, Singapore Environment & Water Industry (EWI) Development Council under award number MEWR 621/06/166 and the Public Utilities Board of Singapore.

Appendix A. Supplementary data

Supplementary data associated with this article can be found, in the online version, at doi:10.1016/j.apcatb.2011.11.009.

References

[1] P. Aldhous, Nature 422 (2003) 251.
[2] M.A. Shannon, P.W. Bohn, M. Elimelech, J.G. Georgiadis, B.J. Marinas, A.M. Mayes, Nature 452 (2008) 301–310.
[3] W.W. Immerzeel, L.P.H.v. Beek, M.F.P. Bierkens, Science 328 (2010) 1382–1385.
[4] B. Bates, Z.W. Kundzewics, S. Wu, J. Palutik, Climate change and water, in: Technical Paper of the Intergovernmental Panel on Climate Change, IPCC Secretariat, Geneva, 2008, 201 pp.
[5] M.N. Chong, B. Jina, C.W.K. Chow, C. Saint, Water Res. 44 (10) (2010) 2997–3027.
[6] D.S. Sholl, J.K. Johnson, Science 312 (2006) 1003–1004.
[7] D.H. Furukawa, Natl. Water Res. Inst. (2008) 1–13.
[8] H. Huang, K. Schwab, J.G. Jacangelo, Environ. Sci. Technol. 43 (9) (2009) 3011–3019.
[9] K. Listiarini, D.D. Sun, J.O. Leckie, J. Membr. Sci. 332 (1–2) (2009) 56–62.
[10] J.G. Jacangelo, R.R. Trussell, M. Watson, Desalination 113 (2–3) (1997) 119–127.
[11] S.S. Madaeni, Water Res. 33 (2) (1999) 301–308.
[12] N. Porcelli, S. Judd, Sep. Purif. Technol. 71 (2010) 137–143.
[13] M. Tomaszewska, S. Mozia, Water Res. 36 (16) (2002) 4137–4143.
[14] Z. Liu, D.D. Sun, P. Guo, J.O. Leckie, Nano Lett. 7 (4) (2007) 1081–1085.
[15] X. Peng, A. Chen, J. Mater. Chem. 14 (2004) 2542–2548.

[16] G. Wang, D. Chen, H. Zhang, J.Z. Zhang, J. Li, J. Phys. Chem. C 112 (2008) 8850–8855.
[17] F.D. Fonzo, C.S. Casari, V. Russo, M.F. Brunella, A.L. Bassi, C.E. Bottani, Nanotechnology 20 (2009) 1–7.
[18] X. Feng, J. Zhai, L. Jiang, Angew. Chem. Int. Ed. 44 (2005) 5115–5118.
[19] Y. Wang, G. Du, H. Liu, D. Liu, S. Qin, N. Wang, C. Hu, X. Tao, J. Jiao, J. Wang, Z.L. Wang, Adv. Funct. Mater. 18 (2008) 1131–1137.
[20] X. Hu, Y. Masuda, T. Ohji, K. Kato, Cryst. Growth Des. 10 (2) (2010) 626–631.
[21] H.Y. Yang, S.F. Yu, S.P. Lau, X. Zhang, D.D. Sun, G. Jun, Small 5 (22) (2009) 2260–2264.
[22] Q. Li, V. Kumar, Y. Li, H. Zhang, T.J. Marks, R.P.H. Chang, Chem. Mater. 17 (2005) 1001–1006.
[23] X. Zhang, A.J. Du, P. Lee, D.D. Sun, J.O. Leckie, Appl. Catal. B: Environ. 84 (1–2) (2008) 262–267.
[24] C. Cheng, B. Liu, H. Yang, W. Zhou, L. Sun, R. Chen, S.F. Yu, J. Zhang, H. Gong, H. Sun, H.J. Fan, ACS Nano 3 (10) (2009) 3069–3076.
[25] M.R. Hoffmann, S.T. Martin, W. Choi, D.W. Bahnemann, Chem. Rev. 95 (1) (1995) 69–96.
[26] R. Ostermann, D. Li, Y. Yin, J.T. McCann, Y. Xia, Nano Lett. 6 (6) (2006) 1297–1302.
[27] X. Feng, L. Feng, M. Jin, J. Zhai, L. Jiang, D. Zhu, J. Am. Chem. Soc. 126 (2003) 62–63.
[28] X. Zhang, J.H. Pan, A.J. Du, W. Fu, D.D. Sun, J.O. Leckie, Water Res. 43 (5) (2009) 1179–1186.
[29] Y. Zhao, X. Zhang, J. Zhai, J. He, L. Jiang, Z. Liu, S. Nishimoto, T. Murakami, A. Fujishima, D. Zhu, Appl. Catal. B: Environ. 83 (2008) 24–29.
[30] H. Zhou, X. Li, T. Fan, F.E. Osterloh, J. Ding, E.M. Sabio, D. Zhang, Q. Guo, Adv. Mater. 22 (2010) 951–956.
[31] X. Li, T. Fan, H. Zhou, S.-K. Chow, W. Zhang, D. Zhang, Q. Guo, H. Ogawa, Adv. Funct. Mater. 19 (2009) 45–56.
[32] T. Zhao, Z. Liu, K. Nakata, S. Nishimoto, T. Murakami, Y. Zhao, L. Jiang, A. Fujishima, J. Mater. Chem. 20 (2010) 5095–5099.
[33] H. Bai, Z. Liu, D.D. Sun, Chem. Commun. 46 (35) (2010) 6542–6544.
[34] S.-H. Choi, G. Ankonina, D.-Y. Youn, S.-G. Oh, J.-M. Hong, A. Rothschild, I.-D. Kim, ACS Nano 3 (9) (2009) 2623–2631.
[35] H. Bai, Z. Liu, D.D. Sun, Phys. Chem. Chem. Phys. 13 (13) (2011) 6205–6210.